








Prospects of Searching for Type Ia Supernovae with 2.5-m Wide Field Survey Telescope

Maokai Hu ^{1,2,*} , Lei Hu ^{1,2} , Ji-an Jiang ^{3,*} , Lin Xiao ^{4,5,6} , Lulu Fan ^{2,6} , Junjie Wei ^{1,2} , Xuefeng Wu ^{1,2} 

¹ Purple Mountain Observatory, Chinese Academy of Sciences, Nanjing 210023, China

² School of Astronomy and Space Sciences, University of Science and Technology of China, Hefei 230026, China

³ National Astronomical Observatory of Japan, National Institutes of Natural Sciences, 2-21-1 Osawa, Mitaka, Tokyo 181-8588, Japan

⁴ Department of Physics, College of Physical Sciences and Technology, Hebei University, Wusidong Road 180, 071002, Baoding, China

⁵ Key Laboratory of High-precision Computation and Application of Quantum Field Theory of Hebei Province, Hebei University, Wusidong Road 180, 071002, Baoding, China

⁶ Department of Astronomy, University of Science and Technology of China, Hefei, 230026, China

* Correspondence: kaihukaihu123@pmo.ac.cn (M. H.); jian.jiang@nao.ac.jp (J. J.)

Abstract: Type Ia Supernovae (SNe Ia) are the thermonuclear explosion of a carbon-oxygen white dwarf (WD) and are well-known as a distance indicator. However, it is still unclear how WDs increase their mass near the Chandrasekhar limit and how the thermonuclear runaway happens. The observational clues associated with these open questions, such as the photometric data within hours to days since the explosion, are scarce. Thus, an essential way is to discover SNe Ia at specific epochs with optimal surveys. The 2.5-m Wide Field Survey Telescope (WFST) is an upcoming survey facility deployed in western China. In this paper, we assess the detectability of SNe Ia with mock observations of WFST. Followed by the volumetric rate, we generate a spectral series of SNe Ia based on a data-based model and introduce the line-of-sight extinction to calculate the brightness from the observer. By comparing with the detection limit of WFST, which is affected by the observing conditions, we can count the number of SNe Ia discovered by mock WFST observations. We expect that WFST can find more than 3.0×10^4 pre-maximum SNe Ia within one-year running. In particular, WFST could discover about 45 bright SNe Ia, 99 early-phase SNe Ia, or 1.1×10^4 well-observed SNe Ia with the hypothesized Wide, Deep, or Medium mode, respectively, suggesting WFST will be an influential facility in time-domain astronomy.

Keywords: type Ia supernovae; general; light curves; telescopes

1. Introduction

Type Ia supernovae (SNe Ia) are the thermonuclear explosion of a carbon-oxygen white dwarf (WD) in a close binary system. Of particular interest is how the WD acquires the mass near the Chandrasekhar limit from its donor star [1]. In the single degenerate scenario, the WD accretes matter from a main-sequence star or red giant through the Roche lobe or stellar wind [2,3]. In contrast, the double degenerate scenario suggests that the donor star is another WD and SNe Ia originate from the merger of the two WDs [4,5]. Cosmologically, SNe Ia serve as a distance indicator based on the luminosity-width relationship [6–8]. The measurements of SNe Ia have exposed the accelerating expansion of the universe and constrained the properties of dark energy [9–11]. Astrophysically, SNe Ia can inject metal elements into interstellar environments and play an important role in galaxy evolution [12–14]. SNe Ia also tightly connect with stellar evolution, accreting process, and merger physics.

To date, the physical nature of SNe Ia, however, is still elusive, such as the pathway of WDs acquiring mass [1], the region of thermonuclear ignition [15], and the existence of a surviving companion or the circumstellar material (CSM) [16,17]. One efficient way to reveal



Citation: Hu, M.; Hu, L.; Jiang, J. et al. Prospects of Searching for Type Ia Supernovae with 2.5-m Wide Field Survey Telescope. *Preprints* **2022**, *1*, 0. <https://doi.org/>

Publisher's Note: MDPI stays neutral with regard to jurisdictional claims in published maps and institutional affiliations.



Copyright: © 2022 by the authors. Licensee MDPI, Basel, Switzerland. This article is an open access article distributed under the terms and conditions of the Creative Commons Attribution (CC BY) license (<https://creativecommons.org/licenses/by/4.0/>).

these mysteries is to capture the multi-band photometric signals of SNe Ia soon after the explosion. Here are several examples:

- The photometric signals within a few hours after the explosion strictly constrain the progenitor of SN 2011fe to be a WD [18].
- The early-phase declining in the ultra-violet bands of iPTF14atg possibly relates to the ejecta-companion interaction [19].
- The early light curve excess and red color evolution of MUSSES 1604D supports the helium burning on the surface of a WD [20].
- The early ultra-violet/optical bump of a large fraction of 91T/99aa-like luminous SNe Ia suggests radioactive decay from abundant ^{56}Ni at the outermost layer of ejecta [21].
- The prominent optical flash within the first day after the explosion points to the presence of ejecta-CSM interaction for SN 2020hvf [22].
- The early-phase observations of SNe 2012cg, 2017cbv, 2018oh, 2019np, 2019yvvq, and 2021aefx are also valuable for studying their physical origins [23–28].

Decades of observational efforts, particularly by virtue of the transient surveys, have been dedicated to exploring the physical nature of SNe Ia and its cosmological applications. The Supernova Legacy Survey discovered about 1,000 SNe Ia from 2003 to 2008, and the redshift is up to 1.0 with the 3.6-meter Canada-France-Hawaii telescope [29]. The Equation of State Supernova Cosmology Experiment program found about 200 SNe Ia with redshift from 0.1 to 0.8 using the 4-meter CTIO Blanco telescope during its 2002-2008 running [30,31]. With the Hubble Space Telescope and the Subaru Hyper Suprime-Cam, the redshift of discovered SNe Ia has been up to above 1.5 [10,32–35]. On the other hand, several supernova surveys are designed to catch the nearby supernovae to investigate their physical nature. The Lick Observatory Supernova Search (LOSS) is a survey project focused on nearby galaxies in the northern sky [36]. After about ten years of running, LOSS discovered 165 SNe Ia with multi-band observations and constructed the explosion rate of SNe Ia in the local universe [37]. The Palomar Transient Factory (PTF) and its successor Zwicky Transient Facility (ZTF) adopted a 1.2-meter Schmidt telescope with a wide field of view to capture time-series signals of SNe Ia [38–40]. For example, PTF 11kx is a SN Ia with ejecta-CSM interaction signals discovered by PTF, and ZTF found a few SNe Ia with early-phase multi-band observations [41,42].

The 2.5-m Wide Field Survey Telescope (WFST) is an upcoming time-domain facility deployed at the Lenghu site of western China [43–47]. The field-of-view of WFST is 6.55 square degrees, and the r -band limiting magnitude with 30-second exposure can reach 22.92 mag, making WFST one of the most powerful imaging survey facilities in the northern hemisphere. WFST can discover SNe Ia in a large distance range, which can be used for both SN science and as cosmological distance indicators. In this paper, we present a preliminary study on the ability of WFST to discover SNe Ia based on mock observations. In Section 2, we introduce the configuration of our framework, including simulations of SNe Ia in the universe, observing conditions of the Lenghu site, and the efficiency of WFST. Section 3 shows the ability of WFST to discover SNe Ia with mock observations. The discussion and conclusion are shown in Section 4.

2. Methods

There are two basics for constructing a framework to simulate SNe Ia observed by WFST. The first one is simulating the brightness of SNe Ia based on their physical properties. The second one is estimating the limiting magnitude of WFST by considering the influence of observing conditions of the Lenghu site. With this framework, we can determine whether WFST can discover SNe Ia at specific phases and distances, and thus estimate the number of discovered SNe Ia by WFST under different observations. To have a reasonable order estimation, we construct a simplified framework without losing any significant factors and describe them sequentially below.

2.1. Simulations of SNe Ia

We randomly generate 10^6 artificial SNe Ia at specific redshifts by following the redshift evolution of the SN Ia rate from Frohmaier et al. (2019) [48]. A data-based model generates the spectra energy distribution of SNe Ia. Considering the time dilation, redshifting, distance, and dust extinction from host galaxies and the Milky Way, we can obtain the multi-band light curves of SNe Ia by convolving WFST filters. Here, we briefly introduce the assumptions adopted in simulating SNe Ia.

The volumetric rate of SNe Ia The volumetric rate of SNe Ia ($r(z)$) is a function of redshift z constrained by the combination of the star-formation history and the delay-time distribution between the short star formation and subsequent SN Ia events. In our study, the redshift of the simulated SNe Ia is less than 1.0 based on the detection limit of WFST. We adopt a power-law distribution to describe the SN Ia rate as $r(z) = r_0 \times (1+z)^\alpha$, where r_0 is the local SN Ia rate with $r_0 = 2.27 \pm 0.19 \times 10^{-5} \text{ Mpc}^{-3} \text{ Year}^{-1}$, and $\alpha = 1.70 \pm 0.21$ from Frohmaier et al. (2019) [48]. Note that we only consider the volumetric rate of normal SNe Ia, excluding the peculiar ones, such as the 91bg-like, 02es-like, Ia-CSM, and super-Chandrasekhar SNe Ia.

The spectral template of SNe Ia SALT3 provides a data-based model to estimate the observer-frame time relating to the peak brightness t_0 , a stretch-like parameter x_1 , a color term c , and a scaling factor x_0 [49]. Inversely, a set of spectra energy distribution of SNe Ia can be generated by SALT3 with predetermined parameters t_0 , x_1 , c , and x_0 [50]. In our study, the parameter t_0 is randomly distributed from one month before to one month after the mock observation run described in Section 2.2. The underlying population of x_1 ($P(x_1)$) is an asymmetric Gaussian distribution as below,

$$P(x_1) = \begin{cases} \exp[-(x_1 - \bar{x}_1)^2/2\sigma_-^2], & \text{if } x_1 \leq \bar{x}_1 \\ \exp[-(x_1 - \bar{x}_1)^2/2\sigma_+^2], & \text{if } x_1 > \bar{x}_1 \end{cases} \quad (1)$$

where $\bar{x}_1 = 0.938 \pm 0.101$, $\sigma_- = 1.551 \pm 0.118$, and $\sigma_+ = 0.269 \pm 0.078$ [51]. The potential distribution of the color term c ($P(c)$) should be a convolution between Gaussian and exponential functions corresponding to the intrinsic scatter of SN Ia color and the extinction from the host galaxy, respectively. For simplicity, we adopt an asymmetric Gaussian function similar to Equation 1 to describe $P(c)$ with $\bar{c} = -0.062 \pm 0.016$, $\sigma_- = 0.032 \pm 0.011$ and $\sigma_+ = 0.25$ [33,51], in which the value of σ_+ is consistent with the previous study on the dust model of SN Ia host galaxies [52]. x_0 is a simple normalization parameter associated with the B -band maximum absolute magnitude of SNe Ia, which has a typical value of -19.31 with a standard deviation of 0.15 [53]. Based on the distributions above, we randomly generate 10,000 sets of these parameters to produce the corresponding spectra energy distribution spanning from -20 days to $+40$ days relative to the peak brightness. Note that the epoch of -20 days is not the explosion time of simulated SNe Ia since the rising time is different under different parameter configurations in the SALT3 model. In our study, the explosion time is roughly estimated by fitting the early-phase light curve with a power-law function [54].

The Milky Way extinction The radiation from SNe Ia goes through the extinction from both their host galaxies and the Milky Way. As discussed above, the color term c has implicitly included the effect of the dust extinction from the host galaxy. Thus, no additional host-galaxy extinction is included. Supernova surveys usually avoid directions toward the galactic disk, so the Milky Way extinction is from the observational data with galactic latitudes $|b| > 10^\circ$ [55].

2.2. The Observing Conditions of Lenghu Site

The Lenghu site is located in the relatively high latitudes of western China, leading to apparent changes in the nighttime and weather conditions during the four seasons. Thus, we divide the whole time window of one-year running into six runs. This time series with six runs

can reasonably deal with the changes in nighttime and weather conditions. Each run has a time window of two adjacent months, with the first consisting of January and February. Thus, WFST could continually monitor the same sky area in each run.

Nighttime Astronomically, nighttime is commonly defined as the sun’s altitude is more than 15 degrees below the horizon. At the Lenghu site, the longest nighttime in winter is about 11.4 hours, and the shortest in summer is only about 5.2 hours. Such noticeable change in the nighttime is unfriendly to the SN survey because the observable time varies daily, and it is difficult to repeatedly monitor the same sky area. By dividing the 1-year observations into six runs, the observable time of each day is the shortest nighttime within the run. Although this simplified process underestimates the observable time of each day, it does guarantee that the telescope can visit the same sky area in each run.

Weather Of the nights at the Lenghu site, there are about 70% photometric time per year [56]. The probability of observable nights in winter is particularly high and relatively low in summer. For simplicity, we use a parameter P_{obs} to describe the probability that a night is observable. In our study, P_{obs} equals 0.8, 0.9, 0.6, 0.4, 0.6, and 0.8 from the first run (January and February) to the last run (November and December), respectively. This approximation satisfies the 70% observable time per year and is consistent with the distribution of observable nights through the accumulated measurement in Lenghu site [56].

Moon phase The full-moon light seriously affects the sky brightness, especially in the optical u and g bands. For simplicity, we adopt the optical r band to simulate the mock observations with WFST. We assume there is no influence on the r -band limiting magnitude during the dark night. The r -band limiting magnitude will be reduced by 0.2 or 0.5 mag during the gray night or bright night, respectively.

2.3. The Efficiency of WFST

The field of view of WFST WFST has a field of view of 6.55 square degrees covered by nine CCDs. However, there are gaps between the CCDs, making the effective field of view ~ 5.95 square degrees.

Limiting magnitude WFST can reach the limiting magnitude of 22.92 in the r band with a 30-second exposure. However, various factors in real observations could reduce this limiting magnitude, including moonlight pollution, atmospheric extinction, and background noise from host galaxies. These effects are not negligible, although they could be reduced by setting a large target-moon distance, observing the sky area near the zenith, and developing more efficient algorithms to eliminate host galaxy contamination using image subtraction. For each simulated observation of WFST, we generate a random number from 0.0 to 1.0 to reduce the r -band limiting magnitude. Such simplification can reasonably reduce the overestimation of discovering SNe Ia by WFST.

2.4. The Configurations of Mock Observations

In this paper, we consider three hypothesized observing modes: wide, medium, and deep observations with the abbreviations ‘Wide’, ‘Medium’, and ‘Deep’, respectively. A summary of the three modes is shown in Table 1. Within an observing run defined in Section 2.2, we assume WFST continuously monitors the pre-selected sky area with the optical r band regardless of the moon phase. The Wide mode aims to cover a large sky area; therefore, the cadence is three days, and there is one visit per night for a specific point. In contrast, daily cadence, two visits per night, and 90-second exposure ensure that the Deep mode can search for SNe Ia in an extensive distance range. The Medium mode is a relatively moderate configuration to a certain degree, in which the cadence is one day, and there is one visit per night.

Table 1. A summary of the three observation modes simulated in this paper.

Observation mode	Filter	Cadence	Visits per night	Exposure	Limiting magnitude
Wide	r	three days	1	30s	22.92
Medium	r	one day	1	30s	22.92
Deep	r	one day	2	90s	23.54

3. Results

For the convenience of comparing the counts of discovered SNe Ia under different hypothesized observing modes, we define the discovery time t_{dis} of SNe Ia as the epoch corresponding to the second r -band observation and the discovery magnitude m_{dis} as the r -band magnitude at the epoch t_{dis} . This definition can reduce contamination from fake sources and moving objects in real observations. On the other hand, purely discovering SN Ia candidates is far from adequate for SN Ia sciences. From the perspective of identifying a supernova candidate, the discovery time t_{dis} is better to be earlier than the peak brightness so that the spectroscopic observation could be triggered at the epoch around the maximum light. To reveal the physical nature of SNe Ia, bright or early-phase ones are still very scarce, while a well-observed light curve is necessary for cosmological distance measurements. Thus, we will investigate the ability to discover SNe Ia at specific epochs with the three mock observations, as shown below.

3.1. Discovering Pre-maximum SNe Ia

Discovering pre-maximum SNe Ia is essential for the SN Ia science, e.g., classification based on the spectrum near the peak light, depicting the spectral evolution covering from early-phase to late-phase epochs, and estimating a stretch-like parameter with a well-observed light curve. However, the rising time of SNe Ia is usually less than 20 days, making discovering pre-maximum SNe Ia difficult.

Transient Name Server (TNS)¹ is a network platform to report transients discovered by worldwide survey programs. Supernova candidates submitted to TNS in 2021 reach about 2.1×10^4 , including all types of supernovae and possibly other transients, such as variables, stellar flares, novae, or active galactic nuclei. Finally, only small proportions could be classified as SNe Ia due to the lack of spectroscopic observations. Nevertheless, the number of supernova candidates counted in TNS still provides an upper limit of the discovered supernovae. As a comparison, Figure 1 shows the m_{dis} distributions of the discovered supernova candidates submitted to TNS in 2021 and the discovered pre-maximum SNe Ia by WFST under the three mock observing modes. These three mock observations can discover above 3.0×10^4 pre-maximum SNe Ia, and the cumulative count reaches 1.5×10^5 for the Wide mode. The peak of the count is at the m_{dis} of 21.9, 22.2, or 22.8 magnitude for the Wide, Medium, or Deep modes, respectively. The magnitude distribution indicates that WFST can search for pre-maximum SNe Ia in a larger distance range or discover local SNe Ia earlier than ongoing survey programs.

With the advent of wide-field time-domain surveys, an enormous number of SNe Ia have been discovered in the last decade. The need for extensive follow-up observations of these transients has quickly overwhelmed the limited spectroscopy resource available. Spectroscopic follow-ups will be a challenge for future WFST surveys. Utilizing machine learning classification based on photometric data can be a promising solution to fully harness the power of the WFST survey [57]. Moreover, optimizing the spectroscopic observations for SNe Ia may help us to efficiently utilize follow-up resources [58].

¹ <https://www.wis-tns.org>

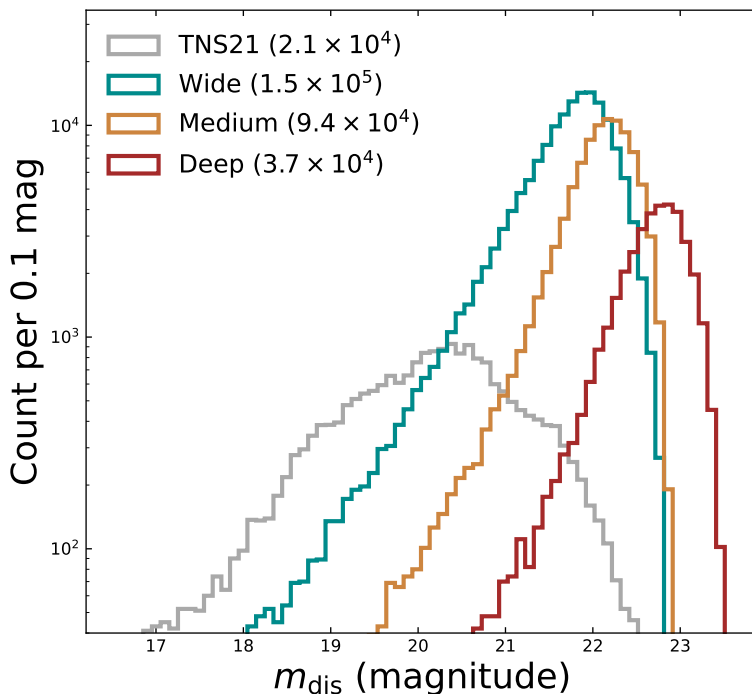


Figure 1. The gray line is the count versus the discovery magnitude (m_{dis}) for supernova candidates submitted to TNS in 2021 (TNS21). The teal, yellow and red lines represent the counts of pre-maximum SNe Ia discovered by WFST under the hypothesized Wide, Medium, and Deep modes, respectively. The corresponding cumulative counts are displayed in the figure legend.

3.2. Discovering Bright SNe Ia

Bright SNe Ia are scarce and valuable, which provide golden samples to be monitored with photometric, spectroscopic, or polarimetric observations. These diverse observations could provide rich clues to the physical origins of SNe Ia. For instance, the asphericity derived from spectropolarimetric diagnostics strongly supports the delayed-detonation explosion of SNe Ia [59,60]. Furthermore, the thermonuclear ignition of carbon-oxygen WDs is off-center, suggested by the relationship between the early-phase velocity gradient of the ejecta and the late-phase velocity shift of emission lines [61]. The late-phase spectroscopic or photometric observations can also diagnose the existence of circumstellar gas around SNe Ia, or the light echos from interstellar or circumstellar dust [17,62,63].

For simplicity, we define bright SNe Ia as the maximum brightness brighter than 16.0 magnitude. As shown in Figure 2, the Wide mode could discover about 45 bright ones earlier than the peak brightness in one-year running, which is comparable to the number discovered in 2021 from the Bright Supernova website². The total number of bright SNe Ia is about 50 per year in the northern sky, estimated with the assumptions such as the SN Ia rate described in Section 2.1, the peak absolute magnitude of -19.3 mag, and moderate dust extinction along the line of sight. Thus, WFST and the running survey facilities can contribute to discovering bright SNe Ia with high completeness.

² <https://www.rochesterastronomy.org/snimages/>

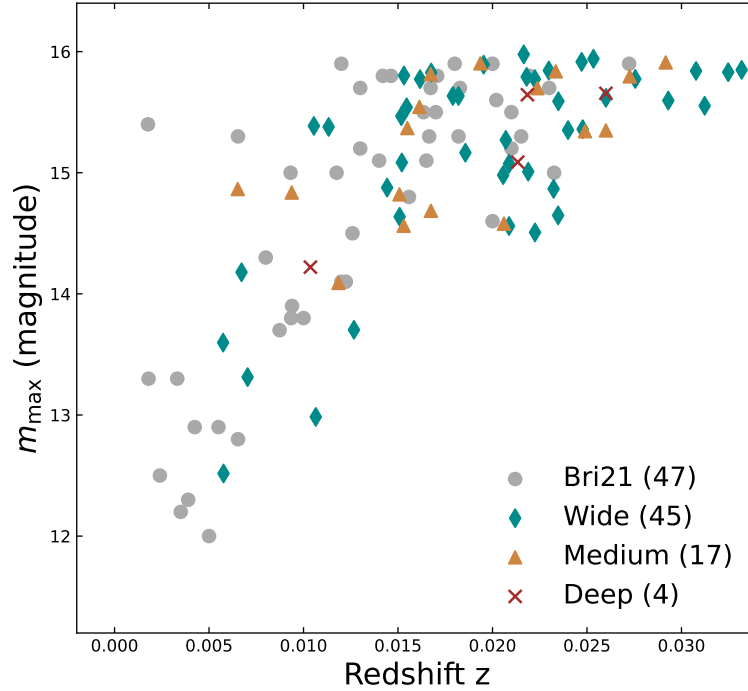


Figure 2. The distributions of the maximum magnitude (m_{\max}) versus redshift z for the bright SNe Ia defined as maximum magnitude brighter than 16.0 mag. The gray symbols are bright SNe Ia discovered in 2021 (Bri21); the rest are the selected bright SNe Ia discovered by WFST under the three mock observations. The total numbers of bright SNe Ia are displayed in the figure legend.

3.3. Discovering Early-phase SNe Ia

The early-phase SNe Ia are full of mysteries and are regarded as a longstanding topic with theoretical or observational views. A ‘dark phase’ might exist between the explosion and the first light due to the adiabatic expansion of the ejecta and the absence of thermal heating from ^{56}Ni decay. This dark phase is an essential observational phenomenon reflecting shallow or deep ^{56}Ni deposit [64], which is determined by the thermonuclear runaway process of WDs. When ignition occurs at the center of a WD, a detonation will destroy the WD and produce a breakout with an X-ray flash [65,66]. Besides, an ultra-violet flash might also be generated from the interaction between the ejecta and an accretion disk [65]. However, these high-energy flashes associated with SNe Ia have not been observed yet.

On the other hand, several SNe Ia events with early-phase photometric observations have shown the clues to the progenitor system or explosion mechanism, such as the helium detonation on the surface of a WD, the mixture of ^{56}Ni to the outer ejecta, and the interaction of the ejecta with a donor star or CSM [19–22,25]. Presently, the early-phase observations of SNe Ia are still rare, limited by the field of view and detection limit of optical facilities and the survey mode. The advantages of WFST can make up for this shortcoming, leading to a potential opportunity for WFST to catch the early-phase signals of SNe Ia.

We define ‘early-phase SNe Ia’ as t_{dis} less than two days since the explosion. Note that t_{dis} is determined by the second observation, thus early-phase SNe Ia cannot be ‘discovered’ by the Wide mode. The upper panel of Figure 3 displays the distribution of discovered early-phase SNe Ia by the hypothesized Deep mode in the space of m_{dis} versus redshift z . Compared with the discovered SNe Ia with early-phase observations from ZTF or other literature [18,19,22–28,42], WFST can find much more early-phase SNe Ia with higher redshift and fainter brightness. Thus, the Deep observation with WFST would contribute a substantial sample of SNe Ia with

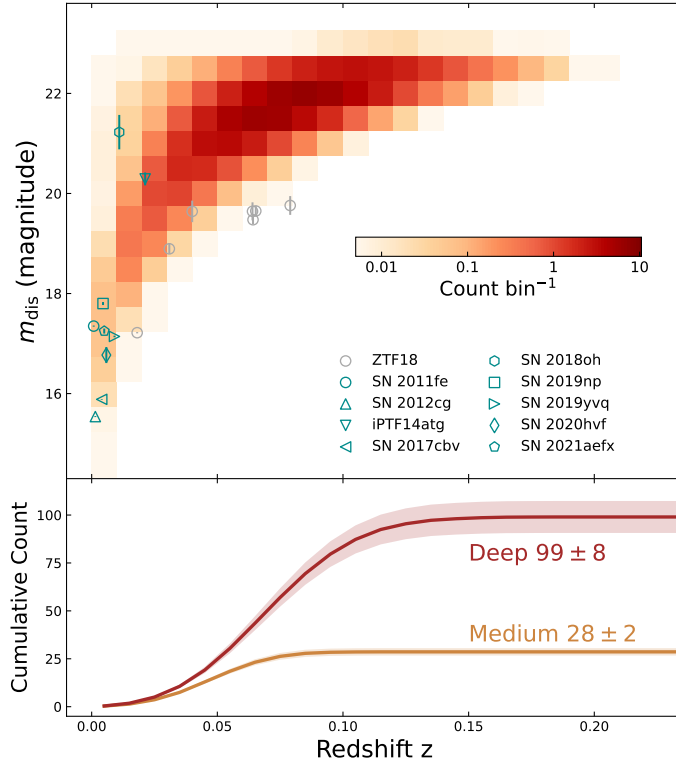


Figure 3. The upper panel displays the distribution of discovery magnitude (m_{dis}) versus z for the discovered early-phase SNe Ia by WFST with the hypothesized Deep mode, in which each bin covers the area of 0.5 mag in m_{dis} and 0.01 in z . The early-phase SNe Ia is defined as t_{dis} less than two days since the explosion. The gray symbols are SNe Ia discovered by ZTF with early-phase observations, and the teal symbols are SNe Ia with early-phase observations from other literature. The solid red line in the lower panel is the corresponding cumulative count of the discovered early-phase SNe Ia with the hypothesized Deep mode. The yellow line represents the Medium mode for comparison. The shadow in the lower panel is the standard deviation in our simulations, which mainly corresponds to the uncertainty of the volumetric rate of SNe Ia.

early-phase photometric data. In comparison, the cumulative count of discovered early-phase SNe Ia by the hypothesized Medium mode is also displayed in the lower panel of Figure 3, which is less than that of the Deep mode. However, catching the signals of early-phase SNe Ia is the first step, and the consequent efforts are also necessary, such as the rapid follow-up observations by other facilities.

3.4. Discovering Well-observed SNe Ia

With the rapid development of transient surveys, the SNe Ia sample has been significantly expanded, and the physical nature of SNe Ia and their cosmological applications have been widely investigated. For instance, nearby SNe Ia can be used to calibrate the Hubble constant H_0 . The latest value of H_0 ($73.04 \pm 1.04 \text{ km s}^{-1} \text{ Mpc}^{-1}$) [67–72] measured from local SNe Ia, calibrated by the Cepheid distance ladder, is in 5σ tension with the predicted H_0 from the cosmic microwave background observations [73–75]. For those SNe Ia at high-redshifts, they can be applied to constrain the property of dark energy [10], test the cosmic distance duality relation [76–78], constrain cosmic opacity [79], estimate the time variation of Newton’s constant G [80], and so on. WFST could discover many well-observed SNe Ia with redshifts above 0.5, providing a vital opportunity for cosmological applications. On the other hand, based on the

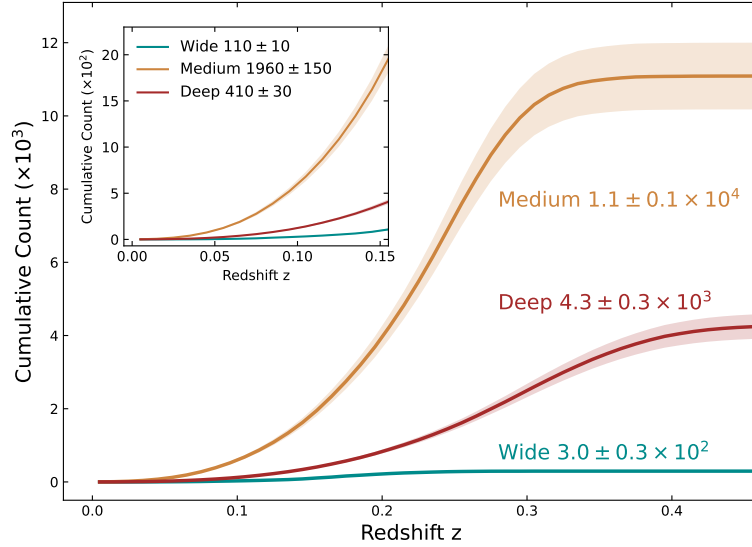


Figure 4. The teal, yellow and red lines are the cumulative counts of discovered well-observed SNe Ia with the hypothesized Wide, Medium, and Deep observations, respectively. The shadows are their corresponding standard deviation due to the uncertainty of the SN Ia rate. The total number of well-observed SNe Ia and the associated standard deviation are also exhibited. The insert figure highlights the cumulative count of SNe Ia at $z < 0.15$.

future sample of the well-observed SNe Ia from WFST, one could also expect the detection of strongly lensed SNe Ia [81]. These events open an exciting possibility to test the Friedman-Lemaître-Robertson-Walker metric [82], investigate the cosmic opacity [83], constrain the speed of light over cosmological distances [84], and measure Hubble constant and cosmic curvature in a model-independent way [85]. However, only two strongly lensed SNe Ia, iPTF16geu [86] and SN Zwicky [87], have been discovered with multiply-imaged observations. Identifying strongly lensed SNe Ia is difficult, as these systems could not be distinguished in the usual optical transient surveys. A photometric method is to select the SNe Ia far brighter than the normal ones as the candidates of strongly lensed SNe Ia [81,88]. WFST could find a certain number of lensed SNe Ia due to the detection capability. However, this part of the exciting forecasting work is beyond the scope of the simulation in this paper. To satisfy the cosmological applications of SNe Ia, we discuss discovering well-observed SNe Ia by WFST in the mock observations.

The well-observed light curve is the primary condition for SNe Ia to be used as a distance indicator because calibrating the peak luminosity of SNe Ia is based on the shape of light curves. It is trivial to define the ‘well-observed light curve’ strictly, but the light curve should be better to cover the whole epochs from the rising phase to the declining phase. Thus, we set up four criteria to select the discovered SNe Ia within the three mock observations:

- t_{dis} is earlier than the peak brightness, which means there are at least two observations during the rising phase of SNe Ia.
- there are at least two nights of observations from -2 days to $+2$ days relative to the peak brightness so that the maximum magnitude can be estimated properly.
- there are at least two nights of observations at the epoch from $+15$ days to $+30$ days after the peak brightness so that the decline of the light curve could be estimated properly.
- there are at least fifteen nights of observations of the whole light curve so that the photometric data is sufficient to derive the light curve parameters.

The cumulative counts of the well-observed SNe Ia discovered by the three hypothesized observing modes are shown in Figure 4. The Medium mode can find $1.1 \pm 0.1 \times 10^4$ well-observed SNe Ia with the redshift up to 0.3. For cosmological use, light curves with at least three filters are necessary to calibrate the photometric magnitude to the standard optical filters in the rest-frame coordinate system and then to estimate rest-frame peak luminosity. By assuming three bands in the mock observations, the number is 650 ± 50 for well-observed SNe Ia within the Hubble flow ($z < 0.15$) under the hypothesized Medium mode, which is larger than the sample used to measure H_0 in previous studies [72]. Thus, SNe Ia search with WFST could play an important role in understanding the Hubble tension.

4. Discussion and Conclusion

In this paper, we constructed a framework to assess the ability of searching for SNe Ia with WFST. However, several factors are not considered, which lead to a larger uncertainty of the estimated number of SNe Ia discovered by WFST under different mock observations, as discussed below.

- Although the dust extinction of host galaxies is already implied in the parameter c of the SALT3 model, it is likely to underestimate the degree of host galaxy extinction. The distribution of the parameter c adopted in our simulations does not correspond to highly reddened SNe Ia. Besides, the extinction law of SN Ia host galaxy may differ from that of the Milky Way, which makes the parameter c incomplete to describe the host galaxy extinction.
- The explosion rate of SNe Ia is likely correlated to the position in host galaxies and varies for different galaxy types. However, the configuration of the explosion rate in this work is only a function of redshift. The over-simplification may bring additional uncertainties into our simulations.
- Detecting a transient close to the center of the host galaxy may involve more difficulties in data processing. The Poisson noise of the host galaxy, as well as the typical artifacts on difference images induced by inaccurate image subtraction or astronomical misalignment [89], can significantly degrade the true detection efficiency in a real survey.
- Although the angular separation between the moon and the pointing of WFST is essential for attenuating moonlight contamination, the separation is ambiguous as the observed sky areas are not specified in the hypothesized modes. For simplicity, we adopt moderate values to account for the influence of the limiting magnitude by moonlight. For the same reason, the airmass is also uncertain, and its influence on the limiting magnitude is attributed to the random number ranging from 0.0 to 1.0.
- We simplified the influence of the weather because the weather can also affect the limiting magnitude, which is not considered in this study.
- The optical r band is the only filter considered in this paper. For observations with more filters, the covered sky area per night should be reduced accordingly.

Nevertheless, our simulations demonstrate the impressive performance of WFST in searching for SNe Ia, as WFST can find over 3.0×10^4 pre-maximum SNe Ia within one-year running under the hypothesized Wide, Medium, or Deep modes. Specifically, the Wide mode has an advantage in discovering bright SNe Ia with a total number of about 45 per year; it is about 99 per year for the discovered early-phase SNe Ia under the Deep mode; the Medium mode can find about 1.1×10^4 SNe Ia with well-observed light curves. Therefore, a concrete observing plan of WFST needs to be determined through comprehensive arguments, such as considering the scientific goals, observing conditions of the Lenghu site, and the operating state of WFST.

Author Contributions: Conceptualization, M.H. and J.J.; methodology, M.H., L.H., J.J., and L.X.; software, M.H.; validation, L.H. and J.J.; resources, L.F., J.W., and X.W.; data curation, M.H.; writing—original draft

preparation, M.H.; writing—review and editing, L.H., J.J., J.W., and L.X.; visualization, M.H.; supervision, X.W.; project administration, M.H., J.J., and X.W.; funding acquisition, X.W. All authors have read and agreed to the published version of the manuscript.

Funding: This research was funded by the National Key Research and Development Programs of China (2022SKA0130100), the National Natural Science Foundation of China (grant Nos. 11725314, and 12041306), the Key Research Program of Frontier Sciences (grant No. ZDBS-LY- 7014) of Chinese Academy of Sciences, the Major Science and Technology Project of Qinghai Province (2019-ZJ-A10), the Natural Science Foundation of Jiangsu Province (grant No. BK20221562), and the China Manned Space Project (CMS-CSST-2021-B11).

Institutional Review Board Statement: Not applicable

Informed Consent Statement: Not applicable

Data Availability Statement: Some data used in this work are available from the published literature.

Acknowledgments: We gratefully thank L. Wang for the instructive comments on the background of Type Ia Supernovae and thank Q. Zhu for providing the information about WFST. Maokai Hu thanks to Jiangsu Funding Program for Excellent Postdoctoral Talent. Lei Hu acknowledges support from Jiangsu Funding Program for Excellent Postdoctoral Talent and China Postdoctoral Science Foundation (Grant No. 2022M723372). Xiao Lin is thankful for the support from National Natural Science Foundation of China (grant No. 12103050), Advanced Talents Incubation Program of the Hebei University, and Midwest Universities Comprehensive Strength Promotion project.

Conflicts of Interest: The authors declare no conflict of interest.

Abbreviations

The following abbreviations are used in this manuscript:

MDPI	Multidisciplinary Digital Publishing Institute
SNe Ia	Type Ia Supernovae
WD	White Dwarf
H_0	Hubble Constant
CSM	Circumstellar Material
LOSS	Lick Observatory Supernova Search
PTF	Palomar Transient Factory
ZTF	Zwicky Transient Facility
WFST	2.5-m Wide Field Survey Telescope

References

1. Maoz, D.; Mannucci, F.; Nelemans, G. Observational Clues to the Progenitors of Type Ia Supernovae. *Annu. Rev. Astron. Astrophys* **2014**, *52*, 107–170, [arXiv:astro-ph.CO/1312.0628]. <https://doi.org/10.1146/annurev-astro-082812-141031>.
2. Whelan, J.; Iben, Icko, J. Binaries and Supernovae of Type I. *Astrophysical Journal* **1973**, *186*, 1007–1014. <https://doi.org/10.1086/152565>.
3. Nomoto, K. Accreting white dwarf models for type I supernovae. I - Presupernova evolution and triggering mechanisms. *Astrophysical Journal* **1982**, *253*, 798–810. <https://doi.org/10.1086/159682>.
4. Iben, I., J.; Tutukov, A.V. Supernovae of type I as end products of the evolution of binaries with components of moderate initial mass. *Astrophysical Journal, Supplement* **1984**, *54*, 335–372. <https://doi.org/10.1086/190932>.
5. Webbink, R.F. Double white dwarfs as progenitors of R Coronae Borealis stars and type I supernovae. *Astrophysical Journal* **1984**, *277*, 355–360. <https://doi.org/10.1086/161701>.
6. Phillips, M.M. The Absolute Magnitudes of Type IA Supernovae. *Astrophysical Journal, Letters* **1993**, *413*, L105. <https://doi.org/10.1086/186970>.
7. Wang, L.; Goldhaber, G.; Aldering, G.; Perlmutter, S. Multicolor Light Curves of Type Ia Supernovae on the Color-Magnitude Diagram: A Novel Step toward More Precise Distance and Extinction Estimates. *Astrophysical Journal* **2003**, *590*, 944–970, [arXiv:astro-ph/0302341]. <https://doi.org/10.1086/375020>.
8. He, S.; Wang, L.; Huang, J.Z. Characterization of Type Ia Supernova Light Curves Using Principal Component Analysis of Sparse Functional Data. *Astrophysical Journal* **2018**, *857*, 110, [arXiv:astro-ph.SR/1802.06125]. <https://doi.org/10.3847/1538-4357/aab0a8>.

9. Riess, A.G.; Filippenko, A.V.; Challis, P.; Clocchiatti, A.; Diercks, A.; Garnavich, P.M.; Gilliland, R.L.; Hogan, C.J.; Jha, S.; Kirshner, R.P.; et al. Observational Evidence from Supernovae for an Accelerating Universe and a Cosmological Constant. *Astronomical Journal* **1998**, *116*, 1009–1038, [arXiv:astro-ph/9805201]. <https://doi.org/10.1086/300499>.
10. Riess, A.G.; Strolger, L.G.; Casertano, S.; Ferguson, H.C.; Mobasher, B.; Gold, B.; Challis, P.J.; Filippenko, A.V.; Jha, S.; Li, W.; et al. New Hubble Space Telescope Discoveries of Type Ia Supernovae at $z \geq 1$: Narrowing Constraints on the Early Behavior of Dark Energy. *Astrophysical Journal* **2007**, *659*, 98–121, [arXiv:astro-ph/0611572]. <https://doi.org/10.1086/510378>.
11. Perlmutter, S.; Aldering, G.; Goldhaber, G.; Knop, R.A.; Nugent, P.; Castro, P.G.; Deustua, S.; Fabbro, S.; Goobar, A.; Groom, D.E.; et al. Measurements of Ω and Λ from 42 High-Redshift Supernovae. *Astrophysical Journal* **1999**, *517*, 565–586, [arXiv:astro-ph/astro-ph/9812133]. <https://doi.org/10.1086/307221>.
12. Matteucci, F.; Greggio, L. Relative roles of type I and II supernovae in the chemical enrichment of the interstellar gas. *Astronomy and Astrophysics* **1986**, *154*, 279–287.
13. Tsujimoto, T.; Nomoto, K.; Yoshii, Y.; Hashimoto, M.; Yanagida, S.; Thielemann, F.K. Relative frequencies of Type Ia and Type II supernovae in the chemical evolution of the Galaxy, LMC and SMC. *Mon. Not. RAS* **1995**, *277*, 945–958. <https://doi.org/10.1093/mnras/277.3.945>.
14. Scannapieco, C.; Tissera, P.B.; White, S.D.M.; Springel, V. Feedback and metal enrichment in cosmological SPH simulations - II. A multiphase model with supernova energy feedback. *Mon. Not. RAS* **2006**, *371*, 1125–1139, [arXiv:astro-ph/astro-ph/0604524]. <https://doi.org/10.1111/j.1365-2966.2006.10785.x>.
15. Höflich, P.; Gerardy, C.L.; Marion, H.; Quimby, R. Signatures of isotopes in thermonuclear supernovae. *NewAR* **2006**, *50*, 470–473. <https://doi.org/10.1016/j.newar.2006.06.074>.
16. González Hernández, J.I.; Ruiz-Lapuente, P.; Tabernero, H.M.; Montes, D.; Canal, R.; Méndez, J.; Bedin, L.R. No surviving evolved companions of the progenitor of SN 1006. *Nature* **2012**, *489*, 533–536, [arXiv:astro-ph.GA/1210.1948]. <https://doi.org/10.1038/nature11447>.
17. Hu, M.; Wang, L.; Wang, X. The Effects of Circumstellar Dust Scattering on the Light Curves and Polarizations of Type Ia Supernovae. *Astrophysical Journal* **2022**, *931*, 110, [arXiv:astro-ph.HE/2109.05504]. <https://doi.org/10.3847/1538-4357/ac6be5>.
18. Nugent, P.E.; Sullivan, M.; Cenko, S.B.; Thomas, R.C.; Kasen, D.; Howell, D.A.; Bersier, D.; Bloom, J.S.; Kulkarni, S.R.; Kandrashoff, M.T.; et al. Supernova SN 2011fe from an exploding carbon-oxygen white dwarf star. *Nature* **2011**, *480*, 344–347, [arXiv:astro-ph.CO/1110.6201]. <https://doi.org/10.1038/nature10644>.
19. Cao, Y.; Kulkarni, S.R.; Howell, D.A.; Gal-Yam, A.; Kasliwal, M.M.; Valenti, S.; Johansson, J.; Amanullah, R.; Goobar, A.; Sollerman, J.; et al. A strong ultraviolet pulse from a newborn type Ia supernova. *Nature* **2015**, *521*, 328–331, [arXiv:astro-ph.SR/1505.05158]. <https://doi.org/10.1038/nature14440>.
20. Jiang, J.A.; Doi, M.; Maeda, K.; Shigeyama, T.; Nomoto, K.; Yasuda, N.; Jha, S.W.; Tanaka, M.; Morokuma, T.; Tominaga, N.; et al. A hybrid type Ia supernova with an early flash triggered by helium-shell detonation. *Nature* **2017**, *550*, 80–83, [arXiv:astro-ph.HE/1710.01824]. <https://doi.org/10.1038/nature23908>.
21. Jiang, J.a.; Doi, M.; Maeda, K.; Shigeyama, T. Surface Radioactivity or Interactions? Multiple Origins of Early-excess Type Ia Supernovae and Associated Subclasses. *Astrophysical Journal* **2018**, *865*, 149, [arXiv:astro-ph.HE/1808.06343]. <https://doi.org/10.3847/1538-4357/aadb9a>.
22. Jiang, J.a.; Maeda, K.; Kawabata, M.; Doi, M.; Shigeyama, T.; Tanaka, M.; Tominaga, N.; Nomoto, K.; Niino, Y.; Sako, S.; et al. Discovery of the Fastest Early Optical Emission from Overluminous SN Ia 2020hvf: A Thermonuclear Explosion within a Dense Circumstellar Environment. *Astrophysical Journal, Letters* **2021**, *923*, L8, [arXiv:astro-ph.HE/2111.09470]. <https://doi.org/10.3847/2041-8213/ac375f>.
23. Marion, G.H.; Brown, P.J.; Vinkó, J.; Silverman, J.M.; Sand, D.J.; Challis, P.; Kirshner, R.P.; Wheeler, J.C.; Berlind, P.; Brown, W.R.; et al. SN 2012cg: Evidence for Interaction Between a Normal Type Ia Supernova and a Non-degenerate Binary Companion. *Astrophysical Journal* **2016**, *820*, 92, [arXiv:astro-ph.SR/1507.07261]. <https://doi.org/10.3847/0004-637X/820/2/92>.
24. Hosseinzadeh, G.; Sand, D.J.; Valenti, S.; Brown, P.; Howell, D.A.; McCully, C.; Kasen, D.; Arcavi, I.; Bostroem, K.A.; Tartaglia, L.; et al. Early Blue Excess from the Type Ia Supernova 2017cbv and Implications for Its Progenitor. *Astrophysical Journal, Letters* **2017**, *845*, L11, [arXiv:astro-ph.HE/1706.08990]. <https://doi.org/10.3847/2041-8213/aa8402>.
25. Dimitriadis, G.; Foley, R.J.; Rest, A.; Kasen, D.; Piro, A.L.; Polin, A.; Jones, D.O.; Villar, A.; Narayan, G.; Coulter, D.A.; et al. K2 Observations of SN 2018oh Reveal a Two-component Rising Light Curve for a Type Ia Supernova. *Astrophysical Journal, Letters* **2019**, *870*, L1, [arXiv:astro-ph.HE/1811.10061]. <https://doi.org/10.3847/2041-8213/aaedb0>.
26. Sai, H.; Wang, X.; Elias-Rosa, N.; Yang, Y.; Zhang, J.; Lin, W.; Mo, J.; Piro, A.L.; Zeng, X.; Andrea, R.; et al. Observations of the very young Type Ia Supernova 2019np with early-excess emission. *Mon. Not. RAS* **2022**, *514*, 3541–3558, [arXiv:astro-ph.HE/2205.15596]. <https://doi.org/10.1093/mnras/stac1525>.
27. Burke, J.; Howell, D.A.; Sarbadhicary, S.K.; Sand, D.J.; Amaro, R.C.; Hiramatsu, D.; McCully, C.; Pellegrino, C.; Andrews, J.E.; Brown, P.J.; et al. A Bright Ultraviolet Excess in the Transitional O2es-like Type Ia Supernova 2019yvvq. *Astrophysical Journal* **2021**, *919*, 142, [arXiv:astro-ph.HE/2101.06345]. <https://doi.org/10.3847/1538-4357/ac126b>.

28. Ashall, C.; Lu, J.; Shappee, B.J.; Burns, C.R.; Hsiao, E.Y.; Kumar, S.; Morrell, N.; Phillips, M.M.; Shahbandeh, M.; Baron, E.; et al. A Speed Bump: SN 2021aefx Shows that Doppler Shift Alone Can Explain Early Excess Blue Flux in Some Type Ia Supernovae. *Astrophysical Journal, Letters* **2022**, *932*, L2, [arXiv:astro-ph.HE/2205.00606]. <https://doi.org/10.3847/2041-8213/ac7235>.
29. Astier, P.; Guy, J.; Regnault, N.; Pain, R.; Aubourg, E.; Balam, D.; Basa, S.; Carlberg, R.G.; Fabbro, S.; Fouchez, D.; et al. The Supernova Legacy Survey: measurement of Ω_M , Ω_Λ and w from the first year data set. *Astronomy and Astrophysics* **2006**, *447*, 31–48, [arXiv:astro-ph/astro-ph/0510447]. <https://doi.org/10.1051/0004-6361:20054185>.
30. Miknaitis, G.; Pignata, G.; Rest, A.; Wood-Vasey, W.M.; Blondin, S.; Challis, P.; Smith, R.C.; Stubbs, C.W.; Suntzeff, N.B.; Foley, R.J.; et al. The ESSENCE Supernova Survey: Survey Optimization, Observations, and Supernova Photometry. *Astrophysical Journal* **2007**, *666*, 674–693, [arXiv:astro-ph/astro-ph/0701043]. <https://doi.org/10.1086/519986>.
31. Foley, R.J.; Matheson, T.; Blondin, S.; Chornock, R.; Silverman, J.M.; Challis, P.; Clocchiatti, A.; Filippenko, A.V.; Kirshner, R.P.; Leibundgut, B.; et al. Spectroscopy of High-Redshift Supernovae from the Essence Project: The First Four Years. *Astronomical Journal* **2009**, *137*, 3731–3742, [arXiv:astro-ph/0811.4424]. <https://doi.org/10.1088/0004-6256/137/4/3731>.
32. Graur, O.; Rodney, S.A.; Maoz, D.; Riess, A.G.; Jha, S.W.; Postman, M.; Dahlen, T.; Holoien, T.W.S.; McCully, C.; Patel, B.; et al. Type-Ia Supernova Rates to Redshift 2.4 from CLASH: The Cluster Lensing And Supernova Survey with Hubble. *Astrophysical Journal* **2014**, *783*, 28, [arXiv:astro-ph.CO/1310.3495]. <https://doi.org/10.1088/0004-637X/783/1/28>.
33. Rodney, S.A.; Riess, A.G.; Strolger, L.G.; Dahlen, T.; Graur, O.; Casertano, S.; Dickinson, M.E.; Ferguson, H.C.; Garnavich, P.; Hayden, B.; et al. Type Ia Supernova Rate Measurements to Redshift 2.5 from CANDELS: Searching for Prompt Explosions in the Early Universe. *Astronomical Journal* **2014**, *148*, 13, [arXiv:astro-ph.CO/1401.7978]. <https://doi.org/10.1088/0004-6256/148/1/13>.
34. Yasuda, N.; Tanaka, M.; Tominaga, N.; Jiang, J.a.; Moriya, T.J.; Morokuma, T.; Suzuki, N.; Takahashi, I.; Yamaguchi, M.S.; Maeda, K.; et al. The Hyper Suprime-Cam SSP transient survey in COSMOS: Overview. *Publications of the ASJ* **2019**, *71*, 74, [arXiv:astro-ph.GA/1904.09697]. <https://doi.org/10.1093/pasj/psz050>.
35. Jiang, J.a.; Yasuda, N.; Maeda, K.; Doi, M.; Shigeyama, T.; Tominaga, N.; Tanaka, M.; Moriya, T.J.; Takahashi, I.; Suzuki, N.; et al. The HSC-SSP Transient Survey: Implications from Early Photometry and Rise Time of Normal Type Ia Supernovae. *Astrophysical Journal* **2020**, *892*, 25, [arXiv:astro-ph.HE/2002.10737]. <https://doi.org/10.3847/1538-4357/ab76cb>.
36. Filippenko, A.V.; Li, W.D.; Treffers, R.R.; Modjaz, M. The Lick Observatory Supernova Search with the Katzman Automatic Imaging Telescope. In Proceedings of the IAU Colloq. 183: Small Telescope Astronomy on Global Scales; Paczynski, B.; Chen, W.P.; Lemme, C., Eds., 2001, Vol. 246, *Astronomical Society of the Pacific Conference Series*, p. 121.
37. Ganeshalingam, M.; Li, W.; Filippenko, A.V.; Anderson, C.; Foster, G.; Gates, E.L.; Griffith, C.V.; Grigsby, B.J.; Joubert, N.; Leja, J.; et al. Results of the Lick Observatory Supernova Search Follow-up Photometry Program: BVRI Light Curves of 165 Type Ia Supernovae. *Astrophysical Journal, Supplement* **2010**, *190*, 418–448. <https://doi.org/10.1088/0067-0049/190/2/418>.
38. Law, N.M.; Kulkarni, S.R.; Dekany, R.G.; Ofek, E.O.; Quimby, R.M.; Nugent, P.E.; Surace, J.; Grillmair, C.C.; Bloom, J.S.; Kasliwal, M.M.; et al. The Palomar Transient Factory: System Overview, Performance, and First Results. *Publications of the ASP* **2009**, *121*, 1395, [arXiv:astro-ph.IM/0906.5350]. <https://doi.org/10.1086/648598>.
39. Rau, A.; Kulkarni, S.R.; Law, N.M.; Bloom, J.S.; Ciardi, D.; Djorgovski, G.S.; Fox, D.B.; Gal-Yam, A.; Grillmair, C.C.; Kasliwal, M.M.; et al. Exploring the Optical Transient Sky with the Palomar Transient Factory. *Publications of the ASP* **2009**, *121*, 1334, [arXiv:astro-ph.CO/0906.5355]. <https://doi.org/10.1086/605911>.
40. Graham, M.J.; Kulkarni, S.R.; Bellm, E.C.; Adams, S.M.; Barbarino, C.; Blagorodnova, N.; Bodewits, D.; Bolin, B.; Brady, P.R.; Cenko, S.B.; et al. The Zwicky Transient Facility: Science Objectives. *Publications of the ASP* **2019**, *131*, 078001, [arXiv:astro-ph.IM/1902.01945]. <https://doi.org/10.1088/1538-3873/ab006c>.
41. Yao, Y.; Miller, A.A.; Kulkarni, S.R.; Bulla, M.; Masci, F.J.; Goldstein, D.A.; Goobar, A.; Nugent, P.; Dugas, A.; Blagorodnova, N.; et al. ZTF Early Observations of Type Ia Supernovae. I. Properties of the 2018 Sample. *Astrophysical Journal* **2019**, *886*, 152, [arXiv:astro-ph.HE/1910.02967]. <https://doi.org/10.3847/1538-4357/ab4cf5>.
42. Bulla, M.; Miller, A.A.; Yao, Y.; Dessart, L.; Dhawan, S.; Papadogiannakis, S.; Biswas, R.; Goobar, A.; Kulkarni, S.R.; Nordin, J.; et al. ZTF Early Observations of Type Ia Supernovae. III. Early-time Colors As a Test for Explosion Models and Multiple Populations. *Astrophysical Journal* **2020**, *902*, 48, [arXiv:astro-ph.HE/2001.00587]. <https://doi.org/10.3847/1538-4357/abb13c>.
43. Lou, Z.; Liang, M.; Yao, D.; Zheng, X.; Cheng, J.; Wang, H.; Liu, W.; Qian, Y.; Zhao, H.; Yang, J. Optical design study of the Wide Field Survey Telescope (WFST). In Proceedings of the Society of Photo-Optical Instrumentation Engineers (SPIE) Conference Series, 2016, Vol. 10154, *Society of Photo-Optical Instrumentation Engineers (SPIE) Conference Series*, p. 101542A. <https://doi.org/10.1117/12.2248371>.
44. Shi, D.D.; Zheng, X.Z.; Zhao, H.B.; Lou, Z.; Wang, H.R.; Qian, Y.; Liu, W.; Yao, D.Z. A Study of Detector Response and Filter Optimization for the Wide Field Survey Telescope. *Acta Astronomica Sinica* **2018**, *59*, 22.
45. Lou, Z.; Liang, M.; Zheng, X.Z.; Xian, H.; Zhang, C.; Zhu, Q.F. Stray light analysis and control for the Wide Field Survey Telescope (WFST). In Proceedings of the Society of Photo-Optical Instrumentation Engineers (SPIE) Conference Series, 2020, Vol. 11445, *Society of Photo-Optical Instrumentation Engineers (SPIE) Conference Series*, p. 114454A. <https://doi.org/10.1117/12.2561485>.
46. Lin, Z.; Jiang, N.; Kong, X. The prospects of finding tidal disruption events with 2.5-m Wide-Field Survey Telescope based on mock observations. *Mon. Not. RAS* **2022**, *513*, 2422–2436, [arXiv:astro-ph.HE/2204.01615]. <https://doi.org/10.1093/mnras/stac946>.

47. Lei, L.; Zhu, Q.; Kong, X.; Wang, T.; Zheng, X.; Shi, D.; Fan, L.; Liu, W. Limiting Magnitude of the Wide Field Survey Telescope (WFST). *Research in Astronomy and Astrophysics* **2022**, *submitted*.
48. Frohmaier, C.; Sullivan, M.; Nugent, P.E.; Smith, M.; Dimitriadis, G.; Bloom, J.S.; Cenko, S.B.; Kasliwal, M.M.; Kulkarni, S.R.; Maguire, K.; et al. The volumetric rate of normal type Ia supernovae in the local Universe discovered by the Palomar Transient Factory. *Mon. Not. RAS* **2019**, *486*, 2308–2320, [arXiv:astro-ph.HE/1903.08580]. <https://doi.org/10.1093/mnras/stz807>.
49. Kenworthy, W.D.; Jones, D.O.; Dai, M.; Kessler, R.; Scolnic, D.; Brout, D.; Siebert, M.R.; Pierel, J.D.R.; Dettman, K.G.; Dimitriadis, G.; et al. SALT3: An Improved Type Ia Supernova Model for Measuring Cosmic Distances. *Astrophysical Journal* **2021**, *923*, 265, [arXiv:astro-ph.CO/2104.07795]. <https://doi.org/10.3847/1538-4357/ac30d8>.
50. Vincenzi, M.; Sullivan, M.; Graur, O.; Brout, D.; Davis, T.M.; Frohmaier, C.; Galbany, L.; Gutiérrez, C.P.; Hinton, S.R.; Hounsell, R.; et al. The Dark Energy Survey supernova programme: modelling selection efficiency and observed core-collapse supernova contamination. *Mon. Not. RAS* **2021**, *505*, 2819–2839, [arXiv:astro-ph.CO/2012.07180]. <https://doi.org/10.1093/mnras/stab1353>.
51. Scolnic, D.; Kessler, R. Measuring Type Ia Supernova Populations of Stretch and Color and Predicting Distance Biases. *Astrophysical Journal, Letters* **2016**, *822*, L35, [arXiv:astro-ph.CO/1603.01559]. <https://doi.org/10.3847/2041-8205/822/2/L35>.
52. Kessler, R.; Becker, A.C.; Cinabro, D.; Vanderplas, J.; Frieman, J.A.; Marriner, J.; Davis, T.M.; Dilday, B.; Holtzman, J.; Jha, S.W.; et al. First-Year Sloan Digital Sky Survey-II Supernova Results: Hubble Diagram and Cosmological Parameters. *Astrophysical Journal, Supplement* **2009**, *185*, 32–84, [arXiv:astro-ph.CO/0908.4274]. <https://doi.org/10.1088/0067-0049/185/1/32>.
53. Barbary, K.; Aldering, G.; Amanullah, R.; Brodwin, M.; Connolly, N.; Dawson, K.S.; Doi, M.; Eisenhardt, P.; Faccioli, L.; Fadeyev, V.; et al. The Hubble Space Telescope Cluster Supernova Survey. VI. The Volumetric Type Ia Supernova Rate. *Astrophysical Journal* **2012**, *745*, 31, [arXiv:astro-ph.CO/1110.6442]. <https://doi.org/10.1088/0004-637X/745/1/31>.
54. Zhang, K.; Wang, X.; Zhang, J.; Zhang, T.; Ganeshalingam, M.; Li, W.; Filippenko, A.V.; Zhao, X.; Zheng, W.; Bai, J.; et al. Optical Observations of the Type Ia Supernova SN 2011fe in M101 for Nearly 500 Days. *Astrophysical Journal* **2016**, *820*, 67, [arXiv:astro-ph.HE/1602.02951]. <https://doi.org/10.3847/0004-637X/820/1/67>.
55. Schlafly, E.F.; Finkbeiner, D.P. Measuring Reddening with Sloan Digital Sky Survey Stellar Spectra and Recalibrating SFD. *Astrophysical Journal* **2011**, *737*, 103, [arXiv:astro-ph.GA/1012.4804]. <https://doi.org/10.1088/0004-637X/737/2/103>.
56. Deng, L.; Yang, F.; Chen, X.; He, F.; Liu, Q.; Zhang, B.; Zhang, C.; Wang, K.; Liu, N.; Ren, A.; et al. Lenghu on the Tibetan Plateau as an astronomical observing site. *Nature* **2021**, *596*, 353–356. <https://doi.org/10.1038/s41586-021-03711-z>.
57. Villar, V.A.; Berger, E.; Miller, G.; Chornock, R.; Rest, A.; Jones, D.O.; Drout, M.R.; Foley, R.J.; Kirshner, R.; Lunnan, R.; et al. Supernova Photometric Classification Pipelines Trained on Spectroscopically Classified Supernovae from the Pan-STARRS1 Medium-deep Survey. *Astrophysical Journal* **2019**, *884*, 83, [arXiv:astro-ph.HE/1905.07422]. <https://doi.org/10.3847/1538-4357/ab418c>.
58. Hu, L.; Chen, X.; Wang, L. Spectroscopic Studies of Type Ia Supernovae Using LSTM Neural Networks. *Astrophysical Journal* **2022**, *930*, 70, [arXiv:astro-ph.HE/2202.02498]. <https://doi.org/10.3847/1538-4357/ac5c48>.
59. Wang, L.; Wheeler, J.C. Spectropolarimetry of supernovae. *Annu. Rev. Astron. Astrophys* **2008**, *46*, 433–474, [arXiv:astro-ph/0811.1054]. <https://doi.org/10.1146/annurev.astro.46.060407.145139>.
60. Cikota, A.; Patat, F.; Wang, L.; Wheeler, J.C.; Bulla, M.; Baade, D.; Höflich, P.; Cikota, S.; Clocchiatti, A.; Maund, J.R.; et al. Linear spectropolarimetry of 35 Type Ia supernovae with VLT/FORS: an analysis of the Si II line polarization. *Mon. Not. RAS* **2019**, *490*, 578–599, [arXiv:astro-ph.HE/1908.07526]. <https://doi.org/10.1093/mnras/stz2322>.
61. Maeda, K.; Benetti, S.; Stritzinger, M.; Röpke, F.K.; Folatelli, G.; Sollerman, J.; Taubenberger, S.; Nomoto, K.; Leloudas, G.; Hamuy, M.; et al. An asymmetric explosion as the origin of spectral evolution diversity in type Ia supernovae. *Nature* **2010**, *466*, 82–85, [arXiv:astro-ph.CO/1006.5888]. <https://doi.org/10.1038/nature09122>.
62. Patat, F.; Chandra, P.; Chevalier, R.; Justham, S.; Podsiadlowski, P.; Wolf, C.; Gal-Yam, A.; Pasquini, L.; Crawford, I.A.; Mazzali, P.A.; et al. Detection of Circumstellar Material in a Normal Type Ia Supernova. *Science* **2007**, *317*, 924, [arXiv:astro-ph/0707.2793]. <https://doi.org/10.1126/science.1143005>.
63. Yang, Y.; Wang, L.; Baade, D.; Brown, P.J.; Cracraft, M.; Höflich, P.A.; Maund, J.; Patat, F.; Sparks, W.B.; Spyromilio, J.; et al. Interstellar-medium Mapping in M82 through Light Echoes around Supernova 2014]. *Astrophysical Journal* **2017**, *834*, 60, [arXiv:astro-ph.HE/1610.02458]. <https://doi.org/10.3847/1538-4357/834/1/60>.
64. Piro, A.L.; Nakar, E. What can we Learn from the Rising Light Curves of Radioactively Powered Supernovae? *Astrophysical Journal* **2013**, *769*, 67, [arXiv:astro-ph.HE/1210.3032]. <https://doi.org/10.1088/0004-637X/769/1/67>.
65. Höflich, P.; Schaefer, B.E. X-ray and Gamma-ray Flashes from Type Ia Supernovae? *Astrophysical Journal* **2009**, *705*, 483–495, [arXiv:astro-ph.HE/0909.1357]. <https://doi.org/10.1088/0004-637X/705/1/483>.
66. Piro, A.L.; Chang, P.; Weinberg, N.N. Shock Breakout from Type Ia Supernova. *Astrophysical Journal* **2010**, *708*, 598–604, [arXiv:astro-ph.HE/0909.2643]. <https://doi.org/10.1088/0004-637X/708/1/598>.
67. Riess, A.G.; Macri, L.; Casertano, S.; Sosey, M.; Lampeitl, H.; Ferguson, H.C.; Filippenko, A.V.; Jha, S.W.; Li, W.; Chornock, R.; et al. A Redetermination of the Hubble Constant with the Hubble Space Telescope from a Differential Distance Ladder. *Astrophysical Journal* **2009**, *699*, 539–563, [arXiv:astro-ph.CO/0905.0695]. <https://doi.org/10.1088/0004-637X/699/1/539>.

68. Riess, A.G.; Macri, L.; Casertano, S.; Lampeitl, H.; Ferguson, H.C.; Filippenko, A.V.; Jha, S.W.; Li, W.; Chornock, R. A 3% Solution: Determination of the Hubble Constant with the Hubble Space Telescope and Wide Field Camera 3. *Astrophysical Journal* **2011**, *730*, 119, [arXiv:astro-ph.CO/1103.2976]. <https://doi.org/10.1088/0004-637X/730/2/119>.
69. Burns, C.R.; Parent, E.; Phillips, M.M.; Stritzinger, M.; Krisciunas, K.; Suntzeff, N.B.; Hsiao, E.Y.; Contreras, C.; Anais, J.; Boldt, L.; et al. The Carnegie Supernova Project: Absolute Calibration and the Hubble Constant. *Astrophysical Journal* **2018**, *869*, 56, [arXiv:astro-ph.CO/1809.06381]. <https://doi.org/10.3847/1538-4357/aae51c>.
70. Riess, A.G.; Casertano, S.; Yuan, W.; Macri, L.; Anderson, J.; MacKenty, J.W.; Bowers, J.B.; Clubb, K.I.; Filippenko, A.V.; Jones, D.O.; et al. New Parallaxes of Galactic Cepheids from Spatially Scanning the Hubble Space Telescope: Implications for the Hubble Constant. *Astrophysical Journal* **2018**, *855*, 136, [arXiv:astro-ph.SR/1801.01120]. <https://doi.org/10.3847/1538-4357/aaadb7>.
71. Riess, A.G.; Casertano, S.; Yuan, W.; Macri, L.M.; Scolnic, D. Large Magellanic Cloud Cepheid Standards Provide a 1% Foundation for the Determination of the Hubble Constant and Stronger Evidence for Physics beyond Λ CDM. *Astrophysical Journal* **2019**, *876*, 85, [arXiv:astro-ph.CO/1903.07603]. <https://doi.org/10.3847/1538-4357/ab1422>.
72. Riess, A.G.; Yuan, W.; Macri, L.M.; Scolnic, D.; Brout, D.; Casertano, S.; Jones, D.O.; Murakami, Y.; Anand, G.S.; Breuval, L.; et al. A Comprehensive Measurement of the Local Value of the Hubble Constant with $1 \text{ km s}^{-1} \text{ Mpc}^{-1}$ Uncertainty from the Hubble Space Telescope and the SH0ES Team. *Astrophysical Journal, Letters* **2022**, *934*, L7, [arXiv:astro-ph.CO/2112.04510]. <https://doi.org/10.3847/2041-8213/ac5c5b>.
73. Planck Collaboration.; Ade, P.A.R.; Aghanim, N.; Armitage-Caplan, C.; Arnaud, M.; Ashdown, M.; Atrio-Barandela, F.; Aumont, J.; Baccigalupi, C.; Banday, A.J.; et al. Planck 2013 results. XVI. Cosmological parameters. *Astronomy and Astrophysics* **2014**, *571*, A16, [arXiv:astro-ph.CO/1303.5076]. <https://doi.org/10.1051/0004-6361/201321591>.
74. Planck Collaboration.; Aghanim, N.; Akrami, Y.; Ashdown, M.; Aumont, J.; Baccigalupi, C.; Ballardini, M.; Banday, A.J.; Barreiro, R.B.; Bartolo, N.; et al. Planck 2018 results. VI. Cosmological parameters. *Astronomy and Astrophysics* **2020**, *641*, A6, [arXiv:astro-ph.CO/1807.06209]. <https://doi.org/10.1051/0004-6361/201833910>.
75. Freedman, W.L. Measurements of the Hubble Constant: Tensions in Perspective. *Astrophysical Journal* **2021**, *919*, 16, [arXiv:astro-ph.CO/2106.15656]. <https://doi.org/10.3847/1538-4357/ac0e95>.
76. Li, Z.; Wu, P.; Yu, H. Cosmological-model-independent Tests for the Distance-Duality Relation from Galaxy Clusters and Type Ia Supernova. *Astrophysical Journal, Letters* **2011**, *729*, L14, [arXiv:astro-ph.CO/1101.5255]. <https://doi.org/10.1088/2041-8205/729/1/L14>.
77. He, Y.; Pan, Y.; Shi, D.P.; Cao, S.; Yu, W.J.; Diao, J.W.; Qian, W.L. Cosmological-model-independent tests of cosmic distance duality relation with Type Ia supernovae and radio quasars. *Chinese Journal of Physics* **2022**, *78*, 297–307, [arXiv:astro-ph.CO/2206.04946]. <https://doi.org/10.1016/j.cjph.2022.06.009>.
78. Xu, B.; Wang, Z.; Zhang, K.; Huang, Q.; Zhang, J. Model-independent Test for the Cosmic Distance-Duality Relation with Pantheon and eBOSS DR16 Quasar Sample. *Astrophysical Journal* **2022**, *939*, 115, [arXiv:astro-ph.CO/2212.00269]. <https://doi.org/10.3847/1538-4357/ac9793>.
79. Wei, J.J. Unbiased Cosmic Opacity Constraints from Standard Sirens and Candles. *Astrophysical Journal* **2019**, *876*, 66, [arXiv:astro-ph.CO/1902.00223]. <https://doi.org/10.3847/1538-4357/ab1587>.
80. Zhao, W.; Wright, B.S.; Li, B. Constraining the time variation of Newton's constant G with gravitational-wave standard sirens and supernovae. *JCAP* **2018**, *2018*, 052, [arXiv:astro-ph.CO/1804.03066]. <https://doi.org/10.1088/1475-7516/2018/10/052>.
81. Goldstein, D.A.; Nugent, P.E.; Goobar, A. Rates and Properties of Supernovae Strongly Gravitationally Lensed by Elliptical Galaxies in Time-domain Imaging Surveys. *Astrophysical Journal, Supplement* **2019**, *243*, 6, [arXiv:astro-ph.GA/1809.10147]. <https://doi.org/10.3847/1538-4365/ab1fe0>.
82. Qi, J.; Cao, S.; Biesiada, M.; Zheng, X.; Ding, X.; Zhu, Z.H. Strongly gravitationally lensed type Ia supernovae: Direct test of the Friedman-Lemaître-Robertson-Walker metric. *Physical Review D* **2019**, *100*, 023530, [arXiv:astro-ph.CO/1802.05532]. <https://doi.org/10.1103/PhysRevD.100.023530>.
83. Ma, Y.B.; Cao, S.; Zhang, J.; Qi, J.; Liu, T.; Liu, Y.; Geng, S. Testing Cosmic Opacity with the Combination of Strongly Lensed and Unlensed Supernova Ia. *Astrophysical Journal* **2019**, *887*, 163, [arXiv:astro-ph.CO/1910.10351]. <https://doi.org/10.3847/1538-4357/ab50c4>.
84. Cao, S.; Qi, J.; Biesiada, M.; Zheng, X.; Xu, T.; Zhu, Z.H. Testing the Speed of Light over Cosmological Distances: The Combination of Strongly Lensed and Unlensed Type Ia Supernovae. *Astrophysical Journal* **2018**, *867*, 50, [arXiv:astro-ph.CO/1810.01287]. <https://doi.org/10.3847/1538-4357/aae5f7>.
85. Qi, J.Z.; Cui, Y.; Hu, W.H.; Zhang, J.F.; Cui, J.L.; Zhang, X. Strongly lensed type Ia supernovae as a precise late-Universe probe of measuring the Hubble constant and cosmic curvature. *Physical Review D* **2022**, *106*, 023520, [arXiv:astro-ph.CO/2202.01396]. <https://doi.org/10.1103/PhysRevD.106.023520>.
86. Goobar, A.; Amanullah, R.; Kulkarni, S.R.; Nugent, P.E.; Johansson, J.; Steidel, C.; Law, D.; Mörtzell, E.; Quimby, R.; Blagorodnova, N.; et al. iPTF16geu: A multiply imaged, gravitationally lensed type Ia supernova. *Science* **2017**, *356*, 291–295, [arXiv:astro-ph.CO/1611.00014]. <https://doi.org/10.1126/science.aal2729>.

-
87. Goobar, A.; Johansson, J.; Schulze, S.; Arendse, N.; Sagués Carracedo, A.; Dhawan, S.; Mörtzell, E.; Fremling, C.; Yan, L.; Perley, D.; et al. SN Zwicky: uncovering a population of gravitational lens galaxies with magnified “standard candles”. *arXiv e-prints* **2022**, p. arXiv:2211.00656, [arXiv:astro-ph.CO/2211.00656].
 88. Goldstein, D.A.; Nugent, P.E. How to Find Gravitationally Lensed Type Ia Supernovae. *Astrophysical Journal, Letters* **2017**, *834*, L5, [arXiv:astro-ph.IM/1611.09459]. <https://doi.org/10.3847/2041-8213/834/1/L5>.
 89. Hu, L.; Wang, L.; Chen, X.; Yang, J. Image Subtraction in Fourier Space. *Astrophysical Journal* **2022**, *936*, 157, [arXiv:astro-ph.IM/2109.09334]. <https://doi.org/10.3847/1538-4357/ac7394>.